Quantitatively predicting modal thermal conductivity of nanocrystalline Si by full-band Monte Carlo simulations

Lina Yang,[1,*] Yi Jiang,[1] and Yanguang Zhou[2,†]
[1]*School of Aerospace Engineering, Beijing Institute of Technology, Beijing 100081, China*
[2]*Department of Mechanical and Aerospace Engineering, The Hong Kong University of Science and Technology, Clear water bay, Kowloon, Hong Kong SAR, China*

(Received 12 July 2021; revised 17 October 2021; accepted 20 October 2021; published 11 November 2021)

Thermal transport in nanocrystalline Si is of great importance for many advanced applications. A better understanding of the modal thermal conductivity of nanocrystalline Si will be expected. In this work, the efficient variance reduced Monte Carlo simulation with full band phonon dispersion is applied to study the modal thermal conductivity of nanocrystalline Si. Importantly, the phonon modal transmissions across the grain boundaries which are modeled by the amorphous Si interface are calculated by the mode-resolved atomistic Green's function method. The predicted ratios of thermal conductivity of nanocrystalline Si to that of bulk Si agree well with that of the experimental measurements in a wide range of grain size. The ratio of thermal conductivity of nanocrystalline Si is decreased from 54% to 3% and the contribution of phonons with mean free path larger than the grain size increases from 30% to 96% as the grain size decreases from 550 to 10 nm. This work demonstrates that the *full band* Monte Carlo simulation using phonon modal transmission by the mode-resolved atomistic Green's function method can effectively capture the phonon transport picture in complex nanostructures, and therefore can provide guidance for designing Si based devices with better performance.

DOI: 10.1103/PhysRevB.104.195303

I. INTRODUCTION

Thermal transport properties of nanostructures are of great importance for advanced applications including thermoelectrics [1,2], microelectronics [3], and thermal barrier coatings [4]. Silicon-based nanostructures are relatively inexpensive, most are nontoxic and stable, which is important for many applications. For example, nanocrystalline Si (nc-Si) based thermoelectrics are used as radio isotope thermoelectricity generator for space missions and nc-Si is also a key component of the commercial polycrystalline silicon photovoltaic solar cells [5]. Thermal transport properties of nc-Si are crucial for improving the efficiency of thermoelectrics or influencing the energy conversion efficiency and lifetime of photovoltaic solar cells. Recent studies have shown that nanocrystalline materials can largely reduce the lattice thermal conductivity (κ), which can largely benefit the efficiency of thermoelectrics [6,7]. Further understanding the thermal transport of nc-Si is necessary for optimizing the performance of devices such as thermoelectrics and photovoltaic solar cells.

In nanocrystalline materials, the remarkable reduction of κ is caused by the impedance of phonons at the grain boundaries when the grain size approaches or is smaller than the phonon mean free path (MFP) [8–11]. Therefore, grain size and phonon transmission at boundaries are two important factors that affect the κ. Wang *et al.* found that κ of nc-Si show a T^2 dependence at low temperature, which cannot be explained by the traditional phonon gray model, further, the frequency dependent (nongray) model should be used for boundary scatterings [8]. A similar phenomena was also found in Si inverse opals [12]. Later, Jugdersuren *et al.* studied nc-Si with grain size decreased to ~10 nm [13]. The study of nc-Si with smaller grain size by molecular dynamic (MD) simulations [9,14] found that the κ is quickly decreased as grain size (<8 nm) decreases, which is caused by the restraining of phonon MFP by the nanograin boundaries [9]. Although there are many works about the thermal transport of nanocrystalline materials, researches based on modal κ analyses are few, which is critical for further understanding the underlying mechanisms of thermal transport.

To quantitatively investigate the phonon modal contribution in nanocrystalline materials, modeling the phonon mode transport process in nanocrystals is required. Phonon Monte Carlo (MC) simulations have been used to study the thermal transport in many complex nanostructures including nanocrystallines [15–18]. Later, the efficiency of traditional phonon MC method is improved by several orders of magnitude by the efficient variance-reduced Monte Carlo (VRMC) algorithm [19,20], which has been widely used in the study of complex structures under the assumption of isotropic phonon dispersion [21,22]. To obtain modal κ, full band phonon dispersion should be used. MC simulations using full band phonon dispersion were applied to study the thermal transport of bulk Si and Si structures [23,24] based on the adiabatic bond charge model and Callaway-Holland model, which found that the correct implementation of phonon dispersion in MC simulations is essential to accurately capture the quasiballistic phonon transport [24]. Full band MC simulation

*yangln@bit.edu.cn
†maeygzhou@ust.hk

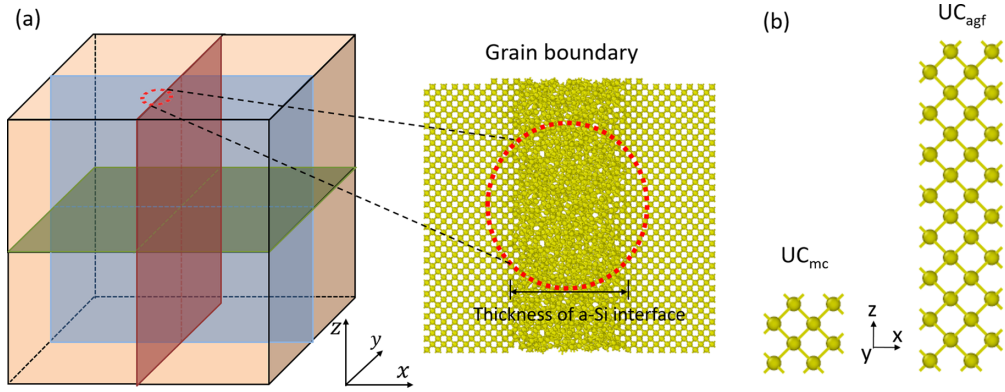

FIG. 1. (a) The schematic of the nanocrystalline Si. The grain boundaries, which are represented by red, blue, and green planes, are perpendicular to the x, y, and z direction, respectively. The red dashed circle shows the zoom-in of the grain boundary, which is modeled by the a-Si interface. (b) The unit cell (UC$_{mc}$) used in the calculation of full band phonon dispersion for the MC simulations and the unit cell (UC$_{agf}$) used in the calculation of phonon modal transmission by the mode-resolved AGF method.

is also used to investigate the thermal transport of Si/Ge heterostructures, however, the phonon transmissions across the interface are calculated by the diffusive mismatch model [25]. Later, the efficient VRMC with full band phonon dispersion using the optimized phonon transmission was applied to study the κ of nc-Si [26]. The calculated κ of nc-Si is quite close to the experimental measurements in a wide range of temperature. The *ab initio* based full band MC simulation was used to study the cross plane κ of Si thin film [27]. Apart from the recent progress of full band MC, using modal level phonon transmission is important to provide a physical and reliable phonon transport picture in nanocrystals.

Many approaches have been applied to calculate the phonon modal transmissions across the interfaces. For instance, the frequency dependent phonon transmission calculated by the spectral diffuse mismatch model [28] was integrated in the MC simulations to calculate the interfacial thermal conductance (ITC). Modal analyses of ITC based on molecular dynamics inherently include the anharmonicity effect, but are hard for large systems due to its high computational requirement [29,30]. On the other hand, the atomistic Green's function (AGF) method is more efficient and easier to be implemented, and therefore has been used extensively to compute the frequency dependent phonon transmission [31–34]. Several extended techniques based on the AGF method have been developed to compute phonon modal transmission [35–38]. A similar numerical method was developed using perfectly matched layer boundaries to compute modal transmission [39]. The scattering boundary method can also calculate the phonon modal transmission [40], which is theoretically equivalent to the AGF method. Recently, Ong and Zhang have extended the conventional AGF formalism to mode-resolved AGF [37], which has been used to calculate the phonon modal transmission across the Si/Ge interface [41] and the amorphous Si (a-Si) interfaces [42]. Although phonon modal transmission by the mode-resolved AGF method has been used to analyze the ITC, few works have integrated it in the κ calculations of nanocrystals.

In this work, the modal κ of nc-Si is investigated by the efficient VRMC with full band phonon dispersion using modal transmission calculated by the mode-resolved AGF method. The grain boundaries are modeled by the a-Si interface. The κ of nc-Si with grain size from 10 nm to 700 nm are calculated, and compared to the experimental works. The thickness of grain boundary which will affect the phonon modal transmission is modulated to study its effect on the κ of nc-Si. Furthermore, the frequency and MFP dependence of κ are analyzed. All the κ of nc-Si are calculated at room temperature.

II. MODEL AND METHOD

A cubic simulation box oriented along the x, y, and z directions as shown in Fig. 1(a) is used to simulate the nc-Si. The periodic heat flux boundary condition [15] along the x direction and a specular boundary condition in the y and z directions are applied, so that the computational domain represents a unit cell which is repeated in all directions. A temperature gradient is applied in the x direction. Three grain boundaries (red, blue, and green planes in Fig. 1) at the center of the simulation box are perpendicular to the x, y, and z direction, respectively. Due to the symmetry boundary conditions, the grain size is the same as the size of the simulation box. The red dashed circle shows the zoom-in of the grain boundary, which is modeled by a-Si interface. The thickness of all the a-Si interfaces is the same in the nc-Si, but it can be modulated for different nc-Si models. The specularity in all the simulations are set as unity, since the a-Si interface is not severely rough and the phonon transmissions have a stronger effect on the κ than specularity [26].

The phonon transport in nc-Si (Fig. 1) is described by the Boltzmann transport equation under the relaxation time approximation. The deviational energy based Boltzmann transport equation [19] is given by

$$\frac{\partial e^d}{\partial t} + \boldsymbol{v}_{\boldsymbol{k},p} \cdot \nabla e^d = \frac{(e^{\mathrm{loc}} - e^{\mathrm{eq}}) - e^d}{\tau(\boldsymbol{k}, p, T)}, \tag{1}$$

where $e^d = \hbar\omega(f - f^{\mathrm{eq}}_{T_{\mathrm{eq}}})$ is the desired deviational distribution function, $\boldsymbol{v}_{\boldsymbol{k},p}$ is the group velocity, $f^{\mathrm{eq}}_{T_{\mathrm{eq}}} = [\exp(\frac{\hbar\omega_{\boldsymbol{k},p}}{k_B T_{\mathrm{eq}}}) - 1)]^{-1}$ is the Bose-Einstein distribution at the control temperature T_{eq}, $\omega_{\boldsymbol{k},p}$ is the angular frequency, and $\tau(\boldsymbol{k}, p, T)$ is the relaxation time. Here $\boldsymbol{k}$ and p denote the wave vector and

polarization of a specific phonon mode, respectively. Equation (1) can be solved by using the linearized version of VRMC algorithm [20]. In MC simulation, 10 648 $\boldsymbol{k}$ points with 24 polarizations are sampled over the entire Brillouin zone. The number of deviational particles is set as $N_{ph} = 8\times10^6$ for each simulation. T_{eq} is set as 300 K. The temperature difference between the two ends of simulation box in x direction is 0.1 K. The grain size can be controlled. The details of the efficient VRMC with full band phonon dispersion, which follow the steps in Refs. [20,26], the temperature profile, and heat flux are shown in Sec. B in the Supplemental Material [43]. Here, only the implementation of grain boundary scattering is briefly shown. The phonon particles can be scattered by internal scattering or the effect of grain boundaries when advect in the simulation domain. When a phonon particle incident happens on a grain boundary, it can be reflected or transmitted which is determined by the phonon modal transmission. First, a random number in standard uniform distribution is drawn, then it is compared with the modal transmission of the incident phonon. If the random number is smaller than the modal transmission, then the phonon is transmitted, otherwise, it is reflected. The specularity of a-Si interface is set as unity in this work, so the phonon wave vector stays the same if the phonon transmits the grain boundary, otherwise the wave vector undergoes specular reflection by the grain boundary.

The full band phonon dispersion and relaxation time of bulk Si used as inputs for the MC simulations, are calculated by SHENGBTE package [44]. Here, the conventional cell (CC) of bulk Si is used as the unit cell (1×1×1 CC, denoted as UC_{mc}) in Fig. 1(b) for the calculation of full band phonon dispersion, which results in 24 polarizations. The interaction between Si atoms is described by the Tersoff potential [45]. The κ of bulk Si is calculated as 239.5 W/m K, which is consistent with the results of MD simulation with the Tersoff potential [46]. The κ based on Tersoff potential is overestimated, but still meaningful for investigating the trend and mechanism of the κ reduction in nanostructures. The phonon group velocities and relaxation time of bulk Si are shown in Sec. A in the Supplemental Material [43].

For the calculation of phonon modal transmission across the grain boundaries (modeled by a-Si interface), the mode-resolved AGF method [37] is applied. The unit cell of the Si contacts is set as 1×4×4 CC (denoted as UC_{agf}) in Fig. 1(b). The Tersoff potential [45] is also used. The a-Si interface which is in the center of the system are generated by melt-quenching method performed in LAMMPS [47], while crystal Si atoms are at the left and right side of the a-Si interface, which is shown in the zoom-in figure in Fig. 1(a). According to the framework of AGF, the system is divided into three parts: the left and right semi-infinite leads (crystal Si) and the interface (a-Si). The equation of motion of the system can be written by the following matrix form : $(\omega^2\mathbf{I} - \mathbf{H})\boldsymbol{\psi} = 0$, where $\mathbf{I}$ is the identity matrix, $\boldsymbol{\psi}$ is the eigenvectors of the whole system, and $\mathbf{H}$ is the dynamical matrix representing the atomic interactions. The frequency interval in all the AGF calculation is 0.1 THz. The key point for the calculation of phonon modal transmission is to construct the mode-resolved transmission matrix $\boldsymbol{t}$. The system is periodic in the y and z directions, therefore, Fourier transform can be applied to the equations of motion following the steps Ref. [37]. The wave vector $\vec{\boldsymbol{k}}_{\parallel}$ (k_y, k_z) is in the plane of y and z. Correspondingly, the mode-resolved transmission matrix $\boldsymbol{t}$ is expressed as $\boldsymbol{t}(\vec{\boldsymbol{k}}_{\parallel})$. For a given $\vec{\boldsymbol{k}}_{\parallel}$, the mode-resolved transmission for mode i with frequency ω on one side of the interface coupled with mode j on the other side of the interface is $\Xi_{ij}(\omega, \vec{\boldsymbol{k}}_{\parallel}) = |t_{ij}(\vec{\boldsymbol{k}}_{\parallel})|^2$. Finally, the modal transmission of phonon mode i can be obtained by summing over all possible phonon modes coupled with mode i, $\Xi_i(\omega, \vec{\boldsymbol{k}}_{\parallel}) = \sum_j \Xi_{ij}(\omega, \vec{\boldsymbol{k}}_{\parallel}) = \sum_j |t_{ij}(\vec{\boldsymbol{k}}_{\parallel})|^2$. The settings of the device and the details of mode-resolved AGF calculation, which follows the steps in Refs. [37,42], are shown in Sec. C in the Supplemental Material [43]. In the following, the mode-resolved AGF method is referred to as AGF for simplicity.

It can be noticed that UC_{mc} and UC_{agf} are 1×1×1 CC and 1×4×4 CC, respectively. Obviously, UC_{agf} is four times the size of UC_{mc} in y and z directions, and the same in the x direction. Therefore, the Brillouin zone (BZ) of UC_{mc} is folded two times in y and z directions, then the folded BZ has the same size as that of UC_{agf}. After folding, the phonon modes of UC_{mc} can be directly compared with that of UC_{agf}, therefore, the phonon modal transmissions of the modes in UC_{mc}, can be directly obtained by linearly interpolating the corresponding modal transmission of the modes in UC_{agf}. Here is the procedure to apply linear interpolation. Firstly, for a given $\vec{\boldsymbol{k}}_{\parallel}$ point in the BZ of UC_{agf}, the phonon dispersion calculated by the mode-resolved AGF method needs to be meshed by frequency and k_x. The frequency is equally meshed, the k_x is meshed by all the different value appearing in the phonon dispersions. Then, at the given $\vec{\boldsymbol{k}}_{\parallel}$ point, for each phonon mode of UC_{mc}, the bin is searched according to its frequency and k_x. After finding the bin, the modal transmission is calculated by linear interpolation of that of the phonon modes at the edges of the bin. According to this procedure, all the phonon modal transmissions are obtained by performing linear interpolation. In the following, the modal transmissions used in the MC simulation are referred to as modal transmissions by interpolation. The details of the BZ folding and the linear interpolation of modal transmission are shown in Sec. D in the Supplemental Material [43].

III. RESULTS

Firstly, the thickness of a-Si interface is set as 5 CC (2.716 nm). The phonon modal transmissions across the a-Si interface which are calculated by the AGF method are shown in Fig. 2(a). The normalized $k_y = 0.167$ and $k_z = 0.167$. The solid black lines calculated by the general utility lattice program (GULP) [48] are shown for leading the eye. The phonon modal transmissions by interpolation are shown in Fig. 2(b), which are obtained by linear interpolation of the modal transmissions in Fig. 2(a). Figure 2(c) shows the phonon modal transmissions by interpolation for all the phonon modes, and the corresponding modal transmissions by the AGF calculations. We find that the phonon modal transmissions are close to unity when the frequency is smaller than 3 THz, and quickly decrease as frequency increase. To investigate the thickness effect of a-Si interface, the phonon modal transmission for a-Si interfaces with thickness of 4 and 6 CC are also

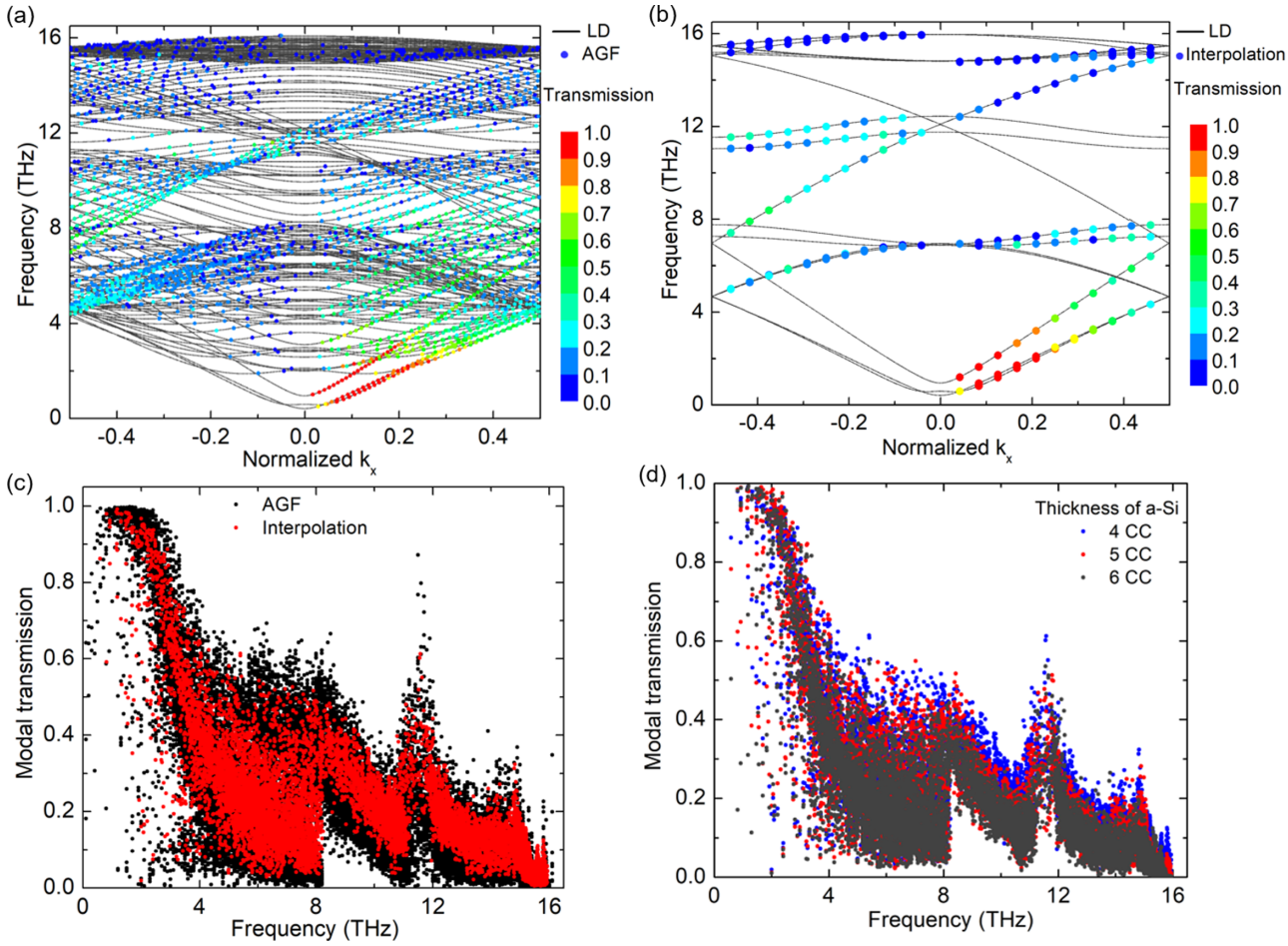

FIG. 2. (a) The phonon modal transmissions calculated by the mode-resolved AGF method (colored dots). The normalized $k_y = 0.167$ and $k_z = 0.167$. The value of transmission is according to the color bar. (b) Phonon modal transmissions by interpolation for the MC simulations (colored dots). The corresponding modal transmissions by the mode-resolved AGF method are these in (a). The black solid lines in (a) and (b) are calculated by lattice dynamics (LD) using GULP [48] for leading the eye. (c) Phonon modal transmission by interpolation for all the phonon modes and the modal transmission by the AGF method. The thickness of a-Si interface is 5 CC (2.716 nm) in (a), (b), and (c). (d) Phonon modal transmissions by interpolation for all the phonon modes across the a-Si interface with thickness of 4 (blue dots), 5 (red dots), and 6 (dark grey dots) CC.

studied. The phonon modal transmissions by interpolation for a-Si interface with thickness of 4 CC (2.172 nm), 5 CC (2.716 nm) and 6 CC (3.259 nm) are shown in Fig. 2(d). It is found that the phonon modal transmissions are slightly decreased at low frequency (<3 THz) and gradually decreased at higher frequency (>3 THz) as the thickness of a-Si increases.

Based on the modal transmission by interpolation in Fig. 2(d), the efficient VRMC with full band phonon dispersion is applied to investigate the thermal transport in nc-Si. Figure 3(a) shows the ratio of κ of nc-Si to that of bulk Si versus the thickness of a-Si interface. For comparison, the experimental results [8] of the nc-Si with grain sizes of 550 and 76 nm are also shown. Interestingly, the predicted ratio of κ agrees well with the experiment results, when the thickness of a-Si interface is 5 CC (2.716 nm) and 4 CC (2.172 nm) for nc-Si with grain size of 550 and 76 nm, respectively. The modal κ of nc-Si and bulk Si are also studied and shown in Fig. 3(b). The modal κ is decreased in the whole frequency range as the grain size decreases. Further, the distribution of phonon MFPs of bulk Si and nc-Si with grain sizes of 550 and 76 nm are compared in Fig. 3(c). It is found that the MFPs of low frequency phonons are much larger than the corresponding grain size because of the large modal transmission [Fig. 2(d)]. Furthermore, the ratios of MFPs of nc-Si to that of bulk Si are studied [Fig. 3(d)], which finds that the phonon MFP can be effectively reduced in the whole frequency range as the grain size decreases.

Furthermore, the spectral κ of bulk Si and nc-Si with the interface thickness of 4, 5, and 6 CC based on the modal κ are shown in Fig. 4(a). For comparison, the corresponding normalized cumulative κ are calculated in Fig. 4(b). Here, the cumulative κ are normalized by the κ of bulk Si. As shown in Fig. 4(a), the contributions of phonon with frequency ranging from 3 to 8 THz in nc-Si is largely reduced because of the reduction of the modal transmission [Fig. 2(d)]. Moreover, as the thickness of a-Si interface increases from 4 CC (2.172 nm) to 6 CC (3.259 nm), the κ of low frequency phonons (<3 THz) is almost unchanged and the overall κ is slightly

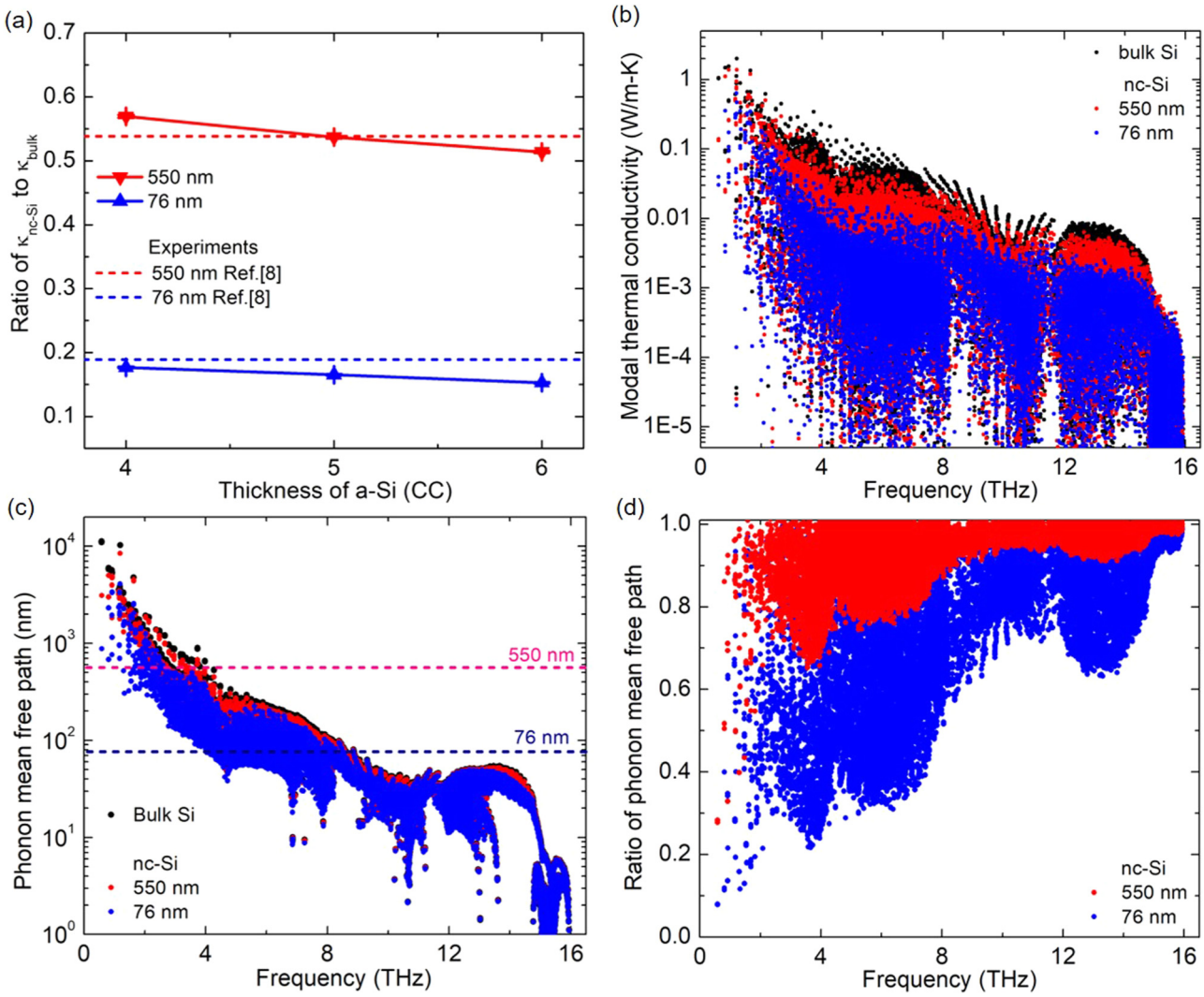

FIG. 3. (a) The ratio of κ of nc-Si ($\kappa_{nc\text{-}Si}$) with grain sizes of 550 nm (red triangle) and 76 nm (blue triangle) to that of bulk Si(κ_{bulk}) versus the thickness of a-Si interfaces 4 CC (2.172 nm), 5 CC (2.716 nm) and 6 CC (3.259 nm). The horizontal red and blue dashed lines represent the experimental measurements [8] for the nc-Si with grain size 550 nm and 76 nm, respectively. (b) The modal κ of nc-Si and bulk Si. (c) The phonon MFP of bulk Si and nc-Si. The pink and blue dashed lines are for reference. (d) The ratios of MFPs of nc-Si to that of bulk Si. In (b) to (d), the nc-Si with grain size 550 and 76 nm are represented by the red and blue dots, respectively.

decreased in Fig. 4(b). To further investigate the grain size effect, the spectral κ of nc-Si with grain size 550 and 76 nm, and the corresponding normalized cumulative κ are shown in Figs. 4(c) and 4(d), respectively. The thickness of a-Si interface is 5 and 4 CC for the nc-Si with grain sizes of 550 and 76 nm, respectively. The results show that as the grain size decreases, the overall κ is largely reduced [Fig. 4(c)] and the ratio of contribution of low frequency phonons is increased [Fig. 4(d)], which indicates that grain size has a strong effect on the κ in the whole frequency range.

To further investigate the grain size effect, nc-Si with grain size varying from 10 to 700 nm are studied. The larger grain size (extended to 5 μm) effect is also provided in Sec. E in the Supplemental Material [43]. The ratio of κ of nc-Si to that of bulk Si versus grain size are shown in Fig. 5(a). For comparison, the experiment measurements of nc-Si with grain sizes 550 nm [8], 144 nm [8], 76 nm [8], 30 nm [49], and 9.7 nm [13] are also shown in Fig. 5(a). We find that the predicted ratio of κ are quite close to that of the experimental measurements when the thickness of a-Si interface is around 5 CC (2.716 nm), which implies that the effect of grain boundary on phonon transport can be reasonably modeled by the a-Si interface. The ratio of κ of nc-Si to that of bulk Si is significantly decreased from 54% to 3% as the grain size decreases from 550 to 10 nm. The normalized cumulative κ versus phonon frequency and phonon mean free path for bulk Si and nc-Si with the grain boundary thickness of 5 CC are shown in Figs. 5(b) and 5(c), respectively. These low frequency phonons (<3 THz) transport substantial amounts of heat in nc-Si by contributing 37%, 46%, 50%, 54% and 57% to the total κ of nc-Si with the grain sizes of 550, 144, 76, 30, and 10 nm, respectively [Fig. 5(b)]. Although the grain size can be reduced to a small value, but the phonon MFPs can be much larger than the grain size [Fig. 3(c)]. As shown in

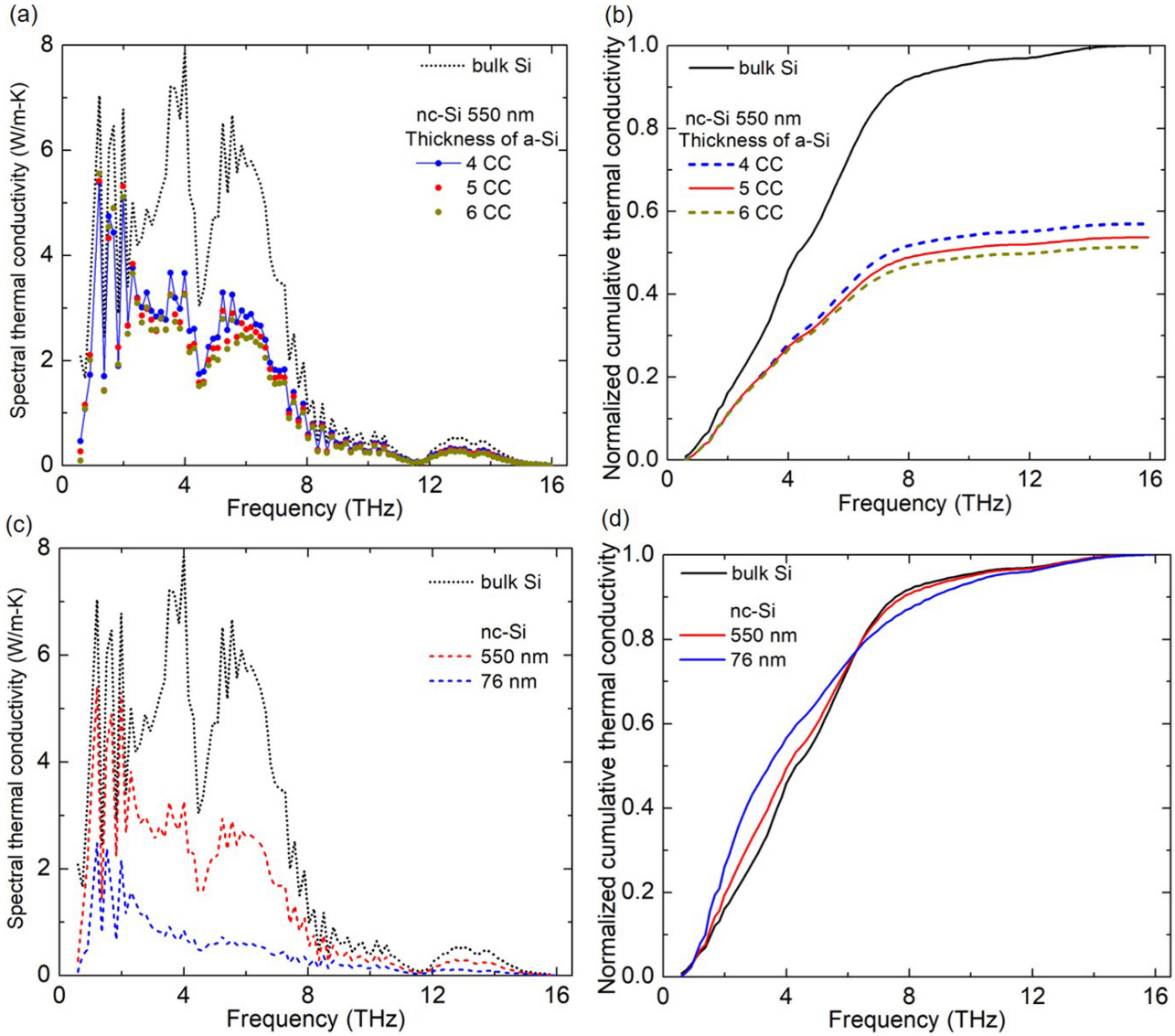

FIG. 4. (a) The spectral κ of bulk Si (black dotted line) and nc-Si with a-Si interface thickness of 4, 5, and 6 CC versus frequency. (b) Normalized cumulative κ of bulk Si and nc-Si versus frequency. The κ of nc-Si is normalized by the κ of bulk Si. The grain size of nc-Si is 550 nm in (a) and (b). (c) The spectral κ of bulk Si (black dotted line) and nc-Si with grain size of 550 nm (red dashed line) and 76 nm (blue dashed line) versus frequency. (d) The normalized cumulative κ of bulk Si and nc-Si with grain sizes of 550 nm (red line) and 76 nm (blue line).

Fig. 5(c), the phonons with MFP larger than the corresponding grain size contribute from 30% to 96% in nc-Si as the grain size decreases from 550 to 10 nm. These analyses indicate that the efficient VRMC with full band phonon dispersion using modal transmission by mode-resolved AGF can effectively predict the ratio of κ of nc-Si which is close to the experimental measurements in a wide range of grain size, and the phonon modes with MFP larger than the grain size transport substantial amounts of heat in nc-Si.

IV. CONCLUSION

In this work, the efficient variance reduced Monte Carlo simulation with full band phonon dispersion using modal transmission by mode-resolved AGF is applied to study the thermal transport in nc-Si. We found that the modal transmission across a-Si interface is close to unity at low frequency (<3 THz) and quickly decreases as the frequency increases. The predicted ratio of κ of nc-Si to that of bulk Si agrees well with the experimental measurements in a wide range of grain size, which is largely decreased from 54% to 3% as the grain size decreases from 550 to 10 nm. The analyses show that the phonon MFP can be reduced in the whole frequency range as the grain size decreases, moreover, the phonons with MFP larger than the corresponding grain size contribute from 30% to 96% in nc-Si as the grain size decreases from 550 to 10 nm. As the thickness of a-Si interface increases from 4 CC (2.172 nm) to 6 CC (3.259 nm), κ of

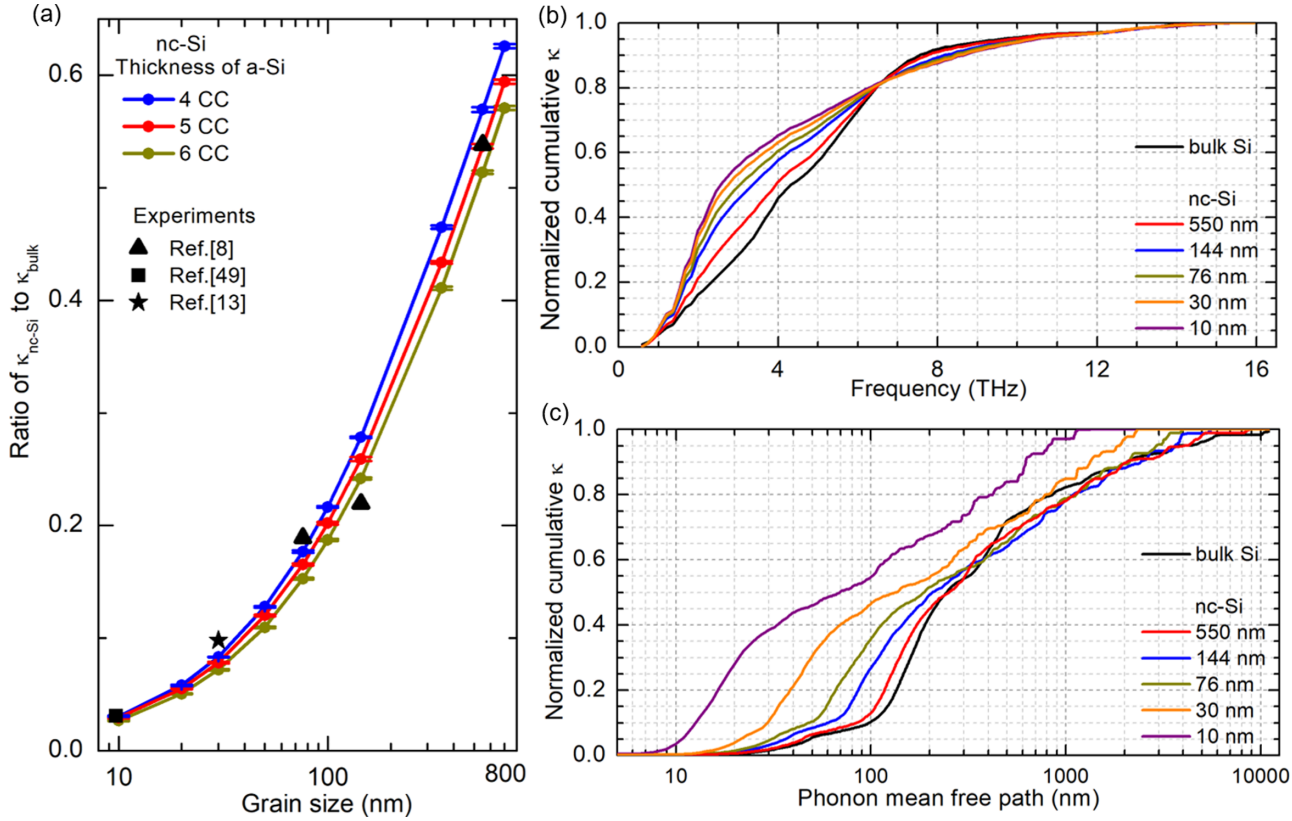

FIG. 5. (a) The ratio of κ of nc-Si to that of bulk Si versus grain size. The thickness of a-Si interface is varied from 4 to 6 CC. The experiment measurements of nc-Si with grain sizes of 550, 144, 76 nm [8] (triangle), 30 nm [49] (star), and 9.7 nm [13] (square) are shown for comparison. The normalized cumulative κ versus frequency (b) and phonon mean free path (c) for bulk Si and nc-Si with grain sizes of 550, 144, 76, 30, and 10 nm. The thickness of a-Si interface is 5 CC in (b) and (c).

nc-Si is slightly reduced. This work demonstrates that the efficient VRMC with full band phonon dispersion using modal transmission by the mode-resolved AGF method can be an effective way to study the modal κ of nc-Si, which can provide deep insight into the thermal transport properties of complex nanostructures.

ACKNOWLEDGMENT

This work was sponsored by the National Natural Science Foundation of China (Grant No. 12004033) and Beijing Institute of Technology Research Fund Program for Young Scholars (L.Y.).

[1] S. He, Y. Li, L. Liu, Y. Jiang, J. Feng, W. Zhu, J. Zhang, Z. Dong, Y. Deng, and J. Luo, Semiconductor glass with superior flexibility and high room temperature thermoelectric performance, Sci. Adv. **6**, eaaz8423 (2020).

[2] J. He and T. M. Tritt, Advances in thermoelectric materials research: Looking back and moving forward, Science **357**, 6358 (2017).

[3] D. G. Cahill, W. K. Ford, K. E. Goodson, G. D. Mahan, A. Majumdar, H. J. Maris, R. Merlin, and S. R. Phillpot, Nanoscale thermal transport, J. Appl. Phys. **93**, 793 (2003).

[4] H.-S. Yang, G.-R. Bai, L. Thompson, and J. Eastman, Interfacial thermal resistance in nanocrystalline yttria-stabilized zirconia, Acta Mater. **50**, 2309 (2002).

[5] D. Bredemeier, D. Walter, S. Herlufsen, and J. Schmidt, Lifetime degradation and regeneration in multicrystalline silicon under illumination at elevated temperature, AIP Adv. **6**, 035119 (2016).

[6] K. Biswas, J. He, I. D. Blum, C.-I. Wu, T. P. Hogan, D. N. Seidman, V. P. Dravid, and M. G. Kanatzidis, High-performance bulk thermoelectrics with all-scale hierarchical architectures, Nature (London) **489**, 414 (2012).

[7] M. Ibánez, Z. Luo, A. Genc, L. Piveteau, S. Ortega, D. Cadavid, O. Dobrozhan, Y. Liu, M. Nachtegaal, and M. Zebarjadi, High-performance thermoelectric nanocomposites from nanocrystal building blocks, Nat. Commun. **7**, 10766 (2016).

[8] Z. Wang, J. E. Alaniz, W. Jang, J. E. Garay, and C. Dames, Thermal conductivity of nanocrystalline silicon: Importance of grain size and frequency-dependent mean free paths, Nano Lett. **11**, 2206 (2011).

[9] S. Ju and X. Liang, Thermal conductivity of nanocrystalline silicon by direct molecular dynamics simulation, J. Appl. Phys. **112**, 064305 (2012).

[10] X. Qian, J. Zhou, and G. Chen, Phonon-engineered extreme thermal conductivity materials, Nat. Mater. **20**, 1188 (2021).
[11] C. Shao, K. Matsuda, S. Ju, Y. Ikoma, M. Kohno, and J. Shiomi, Phonon transport in multiphase nanostructured silicon fabricated by high-pressure torsion, J. Appl. Phys. **129**, 085101 (2021).
[12] J. Ma, B. R. Parajuli, M. G. Ghossoub, A. Mihi, J. Sadhu, P. V. Braun, and S. Sinha, Coherent phonon-grain boundary scattering in silicon inverse opals, Nano Lett. **13**, 618 (2013).
[13] B. Jugdersuren, B. Kearney, D. Queen, T. Metcalf, J. Culbertson, C. Chervin, R. Stroud, W. Nemeth, Q. Wang, and X. Liu, Thermal conductivity of amorphous and nanocrystalline silicon films prepared by hot-wire chemical-vapor deposition, Phys. Rev. B **96**, 014206 (2017).
[14] A. Bodapati, P. K. Schelling, S. R. Phillpot, and P. Keblinski, Vibrations and thermal transport in nanocrystalline silicon, Phys. Rev. B **74**, 245207 (2006).
[15] Q. Hao, G. Chen, and M.-S. Jeng, Frequency-dependent Monte Carlo simulations of phonon transport in two-dimensional porous silicon with aligned pores, J. Appl. Phys. **106**, 114321 (2009).
[16] S. Mazumder and A. Majumdar, Monte Carlo study of phonon transport in solid thin films including dispersion and polarization, J. Heat Transfer **123**, 749 (2001).
[17] M.-S. Jeng, R. Yang, D. Song, and G. Chen, Modeling the thermal conductivity and phonon transport in nanoparticle composites using Monte Carlo simulation, J. Heat Transfer **130**, 042410 (2008).
[18] C. Hua and A. J. Minnich, Importance of frequency-dependent grain boundary scattering in nanocrystalline silicon and silicon–germanium thermoelectrics, Semicond. Sci. Technol. **29**, 124004 (2014).
[19] J.-P. M. Péraud and N. G. Hadjiconstantinou, Efficient simulation of multidimensional phonon transport using energy-based variance-reduced Monte Carlo formulations, Phys. Rev. B **84**, 205331 (2011).
[20] J.-P. M. Péraud and N. G. Hadjiconstantinou, An alternative approach to efficient simulation of micro/nanoscale phonon transport, Appl. Phys. Lett. **101**, 153114 (2012).
[21] N. K. Ravichandran and A. J. Minnich, Coherent and incoherent thermal transport in nanomeshes, Phys. Rev. B **89**, 205432 (2014).
[22] N. G. Dou and A. J. Minnich, Heat conduction in multifunctional nanotrusses studied using Boltzmann transport equation, Appl. Phys. Lett. **108**, 011902 (2016).
[23] K. Kukita and Y. Kamakura, Monte Carlo simulation of phonon transport in silicon including a realistic dispersion relation, J. Appl. Phys. **114**, 154312 (2013).
[24] K. Kukita, I. N. Adisusilo, and Y. Kamakura, Monte Carlo simulation of diffusive-to-ballistic transition in phonon transport, J. Comput. Electron. **13**, 264 (2014).
[25] N. D. Le, B. Davier, P. Dollfus, and J. Saint-Martin, Study of phonon transport across several Si/Ge interfaces using full-band phonon Monte Carlo simulation, arXiv:2102.10833.
[26] L. Yang and A. J. Minnich, Thermal transport in nanocrystalline Si and SiGe by *ab initio* based Monte Carlo simulation, Sci. Rep. **7**, 44254 (2017).
[27] L. Chaput, J. Larroque, P. Dollfus, J. Saint-Martin, and D. Lacroix, *Ab initio* based calculations of the thermal conductivity at the micron scale, Appl. Phys. Lett. **112**, 033104 (2018).
[28] X. Ran, Y. Guo, M. Wang, and M. Transfer, Interfacial phonon transport with frequency-dependent transmissivity by Monte Carlo simulation, Int. J. Heat Mass Transfer **123**, 616 (2018).
[29] K. Gordiz and A. Henry, A formalism for calculating the modal contributions to thermal interface conductance, New J. Phys. **17**, 103002 (2015).
[30] Y. Zhou and M. Hu, Full quantification of frequency-dependent interfacial thermal conductance contributed by two- and three-phonon scattering processes from nonequilibrium molecular dynamics simulations, Phys. Rev. B **95**, 115313 (2017).
[31] W. Zhang, T. Fisher, and N. Mingo, Simulation of interfacial phonon transport in Si–Ge heterostructures using an atomistic Green's function method, J. Heat Transfer **129**, 483 (2007).
[32] W. Zhang, T. Fisher, and N. Mingo, The atomistic Green's function method: An efficient simulation approach for nanoscale phonon transport, Num. Heat Transfer B **51**, 333 (2007).
[33] S. Ju, T. Shiga, L. Feng, Z. Hou, K. Tsuda, and J. Shiomi, Designing Nanostructures for Phonon Transport via Bayesian Optimization, Phys. Rev. X **7**, 021024 (2017).
[34] S. Sadasivam, N. Ye, J. P. Feser, J. Charles, K. Miao, T. Kubis, and T. S. Fisher, Thermal transport across metal silicide-silicon interfaces: First-principles calculations and Green's function transport simulations, Phys. Rev. B **95**, 085310 (2017).
[35] Z. Huang, J. Y. Murthy, and T. S. Fisher, Modeling of polarization-specific phonon transmission through interfaces, J. Heat Transfer **133**, 085310 (2011).
[36] J. C. Klöckner, J. C. Cuevas, and F. Pauly, Transmission eigenchannels for coherent phonon transport, Phys. Rev. B **97**, 155432 (2018).
[37] Z.-Y. Ong and G. Zhang, Efficient approach for modeling phonon transmission probability in nanoscale interfacial thermal transport, Phys. Rev. B **91**, 174302 (2015).
[38] S. Sadasivam, U. V. Waghmare, and T. S. Fisher, Phonon-eigenspectrum-based formulation of the atomistic Green's function method, Phys. Rev. B **96**, 174302 (2017).
[39] R. R. Kakodkar and J. P. Feser, A framework for solving atomistic phonon-structure scattering problems in the frequency domain using perfectly matched layer boundaries, J. Appl. Phys. **118**, 094301 (2015).
[40] S. Lu and A. J. McGaughey, Thermal conductance of graphene/hexagonal boron nitride heterostructures, J. Appl. Phys. **121**, 115103 (2017).
[41] B. Latour, N. Shulumba, and A. J. Minnich, *Ab initio* study of mode-resolved phonon transmission at Si/Ge interfaces using atomistic Green's functions, Phys. Rev. B **96**, 104310 (2017).
[42] L. Yang, B. Latour, and A. J. Minnich, Phonon transmission at crystalline-amorphous interfaces studied using mode-resolved atomistic Green's functions, Phys. Rev. B **97**, 205306 (2018).
[43] See Supplemental Material at http://link.aps.org/supplemental/10.1103/PhysRevB.104.195303 for details about (A) the phonon group velocities and relaxation times of bulk Si; (B) steps of Monte Carlo simulation; (C) settings of the mode-resolved AGF calculation; (D) linear interpolation for obtaining phonon modal transmission; and (E) grain size effect on the thermal conductivity of nc-Si.
[44] W. Li, J. Carrete, N. A. Katcho, and N. Mingo, ShengBTE: A solver of the Boltzmann transport equation for phonons, Comput. Phys. Commun. **185**, 1747 (2014).

[45] J. Tersoff, Modeling solid-state chemistry: Interatomic potentials for multicomponent systems, Phys. Rev. B **39**, 5566 (1989).

[46] S. G. Volz and G. Chen, Molecular-dynamics simulation of thermal conductivity of silicon crystals, Phys. Rev. B **61**, 2651 (2000).

[47] S. Plimpton, Fast parallel algorithms for short-range molecular dynamics, J. Comput. Phys. **117**, 1 (1995).

[48] J. D. Gale and A. L. Rohl, The general utility lattice program (GULP), Mol. Simul. **29**, 291 (2003).

[49] T. Claudio, G. Schierning, R. Theissmann, H. Wiggers, H. Schober, M. M. Koza, and R. P. Hermann, Effects of impurities on the lattice dynamics of nanocrystalline silicon for thermoelectric application, J. Mater. Sci. **48**, 2836 (2013).